2024 I-RIM Conference
October 25-27, Rome, Italy
ISBN: 9788894580556
10.5281/zenodo.14731073

Combining inverse kinematics and rigid constrained dynamics for online collision avoidance

1st Mattia Penzotti
The BioRobotics Institute
Department of Excellence in Robotics and AI
Scuola Superiore Sant'Anna
Pisa, Italy
mattia.penzotti@santannapisa.it

2nd Marco Controzzi
The BioRobotics Institute
Department of Excellence in Robotics and AI
Scuola Superiore Sant'Anna
Pisa, Italy
marco.controzzi@santannapisa.it

***Abstract*—Robots must compute collision-free trajectories on the fly to move proficiently in complex environments, including managing changes over time. In addition, the planner should be able to precisely reproduce the intended trajectory. State-of-the-art local planners are often more conservative in prioritising collision avoidance, typically sacrificing motion accuracy. Here, we propose a novel approach that combines closed-loop inverse kinematics, rigid constrained dynamics, and optimal control to overcome such a limitation. We evaluated its accuracy in simulation, comparing the motion generated near obstacles with that of a state-of-the-art algorithm. while we evaluated its robustness on a real-world bimanual teleoperation platform, including two anthropomorphic grippers. The results suggest that our algorithm can offer a competing alternative in collision-safe sampled motion tracking by achieving superior motion accuracy. In teleoperation, our method proved its efficiency in challenging real-world scenarios.**

***Index Terms*—Collision Avoidance, Inverse Kinematics, Rigid Constrained Dynamics, Optimal Control.**

I. INTRODUCTION

Sampled motion tracking in Cartesian space is fundamental in robotics, particularly in teleoperated systems. To maximise and promote telepresence, the system must retain high fidelity in reproduced motions, while managing the uncertainty of human behaviour, especially in relation to potentially catastrophic collisions [1].

Closed Loop Inverse Kinematics (CLIK) is a top-performing solution in terms of motion tracking accuracy [2]. This class of closed-loop control schemes exhibits desirable properties, such as asymptotic stability and a closed-form solution to the decay of tracking errors [3]. Additionally, in the case of redundant kinematic chains, null space projection techniques can significantly augment the Cartesian space control scheme by simultaneously attaining lower priority tasks (e.g. achieving minimum distance from a default posture) [4]. However, avoiding collisions is a top priority during motion tracking in Cartesian space. In this context, null space projection techniques cannot guarantee adequate hardware safety against collisions [5]. Concerning collisions, the most popular solution is to exploit multi-objective optimisation with gradient descent. The main idea is to combine attractive potential fields, with the end-effector target pose at the minimum of the gradient, and repulsive fields, surrounding obstacle geometries [6]. Typically, its influence decreases quadratically with respect to the distance from the obstacle [7]. The main drawback is that the accuracy of the motion is often compromised inexplicably in the proximity of the obstacle boundaries [8]. As a result, expert intuition or statistical approaches are required to properly tune important parameters to achieve satisfactory tracking accuracy while maintaining a certain level of collision safety [9]. However, in multi-objective optimisation settings, specific balances between accuracy and safety could be unattainable [10].

In the present work, we propose a novel approach to local motion synthesis which solves the problem of collision avoidance while maintaining high pose tracking fidelity. As a main contribution, we incorporate collision safety into a closed-loop inverse kinematics control scheme, leveraging constrained rigid body dynamics to accurately predict near-future physically plausible states for articulated serial chains [11]. The main benefit is that non-compenetration constraints can be precisely enforced between manipulator links and any collision shape by defining a minimum allowable distance ρ_0, which we call the *clearance* value. Depending on task requirements and uncertainties in estimating the shape or pose of known obstacles and manipulator links, any desired level of clearance between them can be easily regulated, even at runtime. In simulation, we proved effectiveness in collision avoidance and pose tracking fidelity by comparing with a state-of-the-art method. Through intensive experiments conducted on a bimanual teleoperation platform, we proved this algorithm to be capable of handling complex real-world scenarios with demanding accuracy requirements.

II. METHOD

A. Background

We consider an articulated serial chain, articulation, for short, with n links and a generic number of obstacles. Given its state $\mathbf{q}(t), \dot{\mathbf{q}}(t)$ in the configuration space with reduced

Marco Controzzi and Mattia Penzotti are supported by the European Commission under the Horizon 2020 programme for Research and Innovation (project acronym: APRIL, project number: 870142) and by the Italian Ministry of Research, under the PNNR action "THE-Tuscany Health Ecosystem" – Spoke 9 (project number ECS 00000017).

coordinates, we consider $X(\mathbf{q}(t))$ and $V(\dot{\mathbf{q}}(t))$ the centres of mass positions and velocities such that both are $6n$-by-1 maximal coordinate vectors.

$X(t)$ —we drop dependency on joint state when clear—can be easily computed by applying forward kinematics and $V(t)$ through the articulation Jacobians. Generally speaking, our aim is to derive a physically plausible state X^+ and V^+ at time $t+T$ applying the Euler symplectic scheme, such that

$$X^+ = X + V^+ T \tag{1}$$

where we utilised the superscripts to drop the dependency on time.

For any number of potential collision pairs, we can identify one (or more if the shapes are non-convex) distance normal $\mathbf{n}$. The set $\mathcal{N} = \{\mathbf{n}_1, \ldots, \mathbf{n}_s\}$ collects all the normals where the distance is less than or equal to ρ_0 so that we can achieve collision safety by incorporating at this stage the *clearance* parameter. An s-by-1 vector $C_{\mathcal{N}}$ collects the measured compenetrations.

An articulation is said to be in collision whenever the set $\mathcal{N}$ is not empty. A Baumgarte correction scheme [11] updates the centres of mass velocities to produce proper separation effects

$$J_{\mathcal{N}} V^+ = -\beta C_{\mathcal{N}} \tag{2}$$

where $J_{\mathcal{N}}$ represents the s-by-$6n$ constraints Jacobian, which, for any link found in a collision, maps a velocity update at the contact point to a velocity change at the centre of mass.

Without external forces, the constrained equations of motion are

$$\left(V^+ - V\right) T^{-1} = M^{-1} J_{\mathcal{N}}^\top \lambda \tag{3}$$

where λ represents an unknown s-by-1 vector of contact forces (or constraint multipliers) and $M(\mathbf{q})$ is the articulated body inertia tensor [12]. According to (2)

$$\left(-\beta C_{\mathcal{N}} - J_{\mathcal{N}} V\right) T^{-1} = J_{\mathcal{N}} M^{-1} J_{\mathcal{N}}^\top \lambda \tag{4}$$

where we call η the left-hand side and $G = J_{\mathcal{N}} M^{-1} J_{\mathcal{N}}^\top$ the so-called Delassus matrix. Constraint forces can only act in a repulsive fashion leading to condition $\lambda \geq 0$, thus leading to the linear complementarity problem

$$w = G\lambda - \eta \qquad\qquad 0 = w \perp \lambda \geq 0 \tag{5}$$

Once we solve (5) with the Projected Gauss-Seidel iterative method [11] to determine λ, we can make use of (3) and (1) to derive the physically plausible state

$$X^+ = X + VT + M^{-1} J_{\mathcal{N}}^\top T^2 \lambda \tag{6}$$

B. Combining constrained dynamics and inverse kinematics

Our main contribution resides in the way we leverage rigid constrained dynamics to predict the physical plausibility of inverse kinematics solutions. The resulting control scheme in Fig. 1 can be thought of as the cascade composition of three major actors: a CLIK-based regulator, a Constrained Dynamics Solver (CDS) and a feedback Optimal Controller (OC) [13].

Closed-loop inverse kinematics typically involves the instantaneous regulation of joint space velocities set-point $\dot{\mathbf{q}}_d$ to

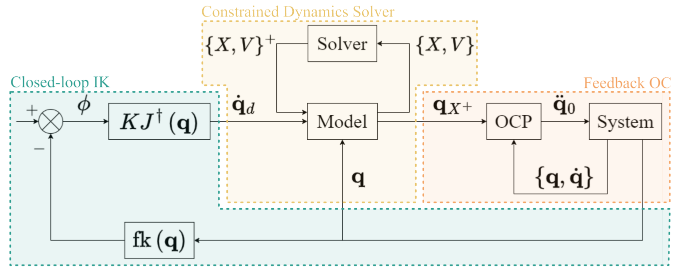

Fig. 1: The control scheme of our method

ensure an exponentially decaying regulation error $\phi(t)$ in the task space

$$\dot{\mathbf{q}}_d = K J^\dagger \phi + B\left(\tilde{\mathbf{q}} - \mathbf{q}\right) \tag{7}$$

where $J^\dagger$ denotes the Moore-Penrose pseudo-inverse of the articulation Jacobian [14] and K is a diagonal matrix of positive scalar gains. The null-space projection operator $B = \left(I - J^\dagger J\right)$ is used to resolve redundancy by defining some default posture attractor $\tilde{\mathbf{q}}$ with respect to current joint positions $\mathbf{q}$.

Given $X(\mathbf{q})$ and $V(\dot{\mathbf{q}}_d)$, we can make use of (6) to predict a physically plausible state X^+ at time $t+T$, where we call T the prediction horizon. We bring the solution from maximal to reduced coordinates with the operator $\mathbf{q}\left(X^+\right)$. We will simply use $\mathbf{q}_{X^+}$, for a more compact notation.

Before collecting the set of contacts $\mathcal{N}$ on which the CDS operates, we can perform a comprehensive set of updates to the collision scene, including the estimated shape of the articulation links, which can serve the purpose of updating runtime collision shapes that are rigidly connected to the serial chain. Examples include grasped objects or even grippers.

The feedback OC drives the serial chain from the current $\{\mathbf{q}, \dot{\mathbf{q}}\}$ to the final $\{\mathbf{q}_{X^+}, 0\}$ kinematic state by minimizing the joint accelerations $\ddot{\mathbf{q}} \equiv \mathbf{u}$. In particular, we solve the Optimal Control Problem (OCP)

$$\begin{aligned}
&\min_{\mathbf{u}(t)} \quad \int_0^T \mathbf{u}(t)^\top \mathbf{u}(t)\, dt \quad \text{subject to:} \\
&\mathbf{x}(t) = \begin{bmatrix} \mathbf{p}(t) \\ \mathbf{v}(t) \end{bmatrix}, \quad \dot{\mathbf{x}}(t) = \begin{bmatrix} \mathbf{v}(t) \\ \mathbf{u}(t) \end{bmatrix}, \quad t \in [0, T] \\
&\mathbf{x}(0) = \begin{bmatrix} \mathbf{q} \\ \dot{\mathbf{q}} \end{bmatrix}, \quad \mathbf{x}(T) = \begin{bmatrix} \mathbf{q}_{X^+} \\ 0 \end{bmatrix}
\end{aligned}$$

Our experience suggests that ignoring $\dot{\mathbf{q}}_{V^+}$ from the CDS solution can prevent joint velocity artefacts (e.g. due to discontinuities in the CDS solution). It can be proved that the solution is a differential equation of the form $\mathbf{p}^{(4)} = 0$, where $\mathbf{p}^{(4)}$ is the fourth derivative of $\mathbf{p}(t)$, with a third-order polynomial as a general solution. By imposing initial and terminal constraints on the third-order polynomial, we derive the optimal control action $\ddot{\mathbf{q}}_0 = -\frac{2}{T^2}\left(3\mathbf{q} - 3\mathbf{q}_{X^+} + 2T\dot{\mathbf{q}}\right)$. Finally, we obtain joint velocities—for control—with symplectic Euler integration.

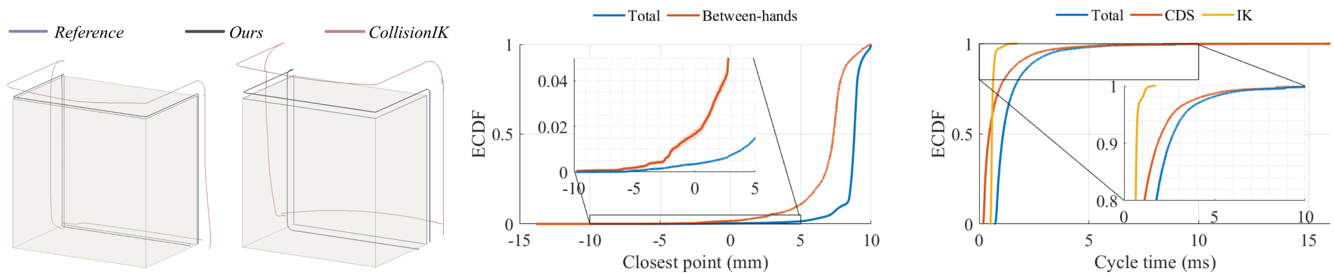

(a) (b) (c)

Fig. 2: a) Traced paths, with *clearance* parameter set to 5 and 15 mm. The path start and end points are on the lower right corner of the obstacle, while the robot tool flange is always tangent to the surface. b) Closest point distance on clearance violations during the bi-manual platform experiment. The Empirical Cumulative Distribution Function (ECDF) is represented with 95% confidence bounds. `Between-hands` represents clearance violation occurring at the interaction between fingers of the two anthropomorphic grippers. c) Computational cost ECDF with 95% confidence bounds on the bi-manual teleoperation platform. The total is composed of constrained dynamics solve time (CDS) and inverse kinematics computation time (IK).

III. Experiments and Results

A. Obstacle circumnavigation

To assess the quality of the proposed motion synthesis method, we select a 6-axis Universal Robots UR10e serial manipulator as a simulated robotic platform.

We compare:

- Our approach —loop rate 125 Hz, $T = 0.2s$;
- A state-of-the-art multi-objective optimisation approach (*CollisionIK*) [7]—loop rate 3 kHz.

The setup consists of the robot itself, standing on an elevated base, and a prismatic collision element—size 36×24×36 cm, centred at coordinates {0,-0.8,0} w.r.t. the robot base (metres).

As a reference trajectory, we choose a series of time-parameterized way points that are exactly positioned on the obstacle surface. We interleave translations and rotations so that while moving near the obstacle, the robot flange is always tangent to the obstacle surface. We consider three levels of the *clearance* parameter, which is equivalently defined in *CollisionIK* as the cutoff distance between collision and non-collision [7].

We define the error in the accuracy of a trajectory as the difference between the reference and the solution computed by our algorithm or the *CollisionIK* method, which are enriched with collision avoidance policies. In particular, we measure the magnitude of the error in position e_p and the magnitude of the error in linear velocities e_v. We report median values (mm and mm/s) and interquartile range (IQR). We do not report angular errors, less than 0.1° and 0.1° per second, given that the nominal trajectories are mostly composed of translations only.

A qualitative picture of the performance of the two methods is reported in Fig. 2a, while quantitative results are presented in Table I. With our algorithm, the median value e_p is generally equal to the clearance parameter ρ_0, indicating that the robot end effector tracks the reference trajectory as precisely as possible while respecting the clearance value required, which acts as a safety margin by defining the minimum distance allowed from the obstacle surface.

TABLE I: Results of the simulation experiment

	Our algorithm		*CollisionIK*	
Clearance	e_p	e_v	e_p	e_v
5	5 ± 1.1	0.3 ± 2.2	37.2 ± 0.7	2.4 ± 8.1
10	9.8 ± 0.3	0.5 ± 4.7	60.2 ± 0.6	5.6 ± 14
15	15 ± 1.2	0.9 ± 7.1	80.6 ± 1	6.7 ± 15.4

In contrast, the *CollisionIK* solver typically exhibits e_p values which differ broadly from the clearance value. Moreover, from the high e_v median and IQR values, it can be observed that in the case of *CollisionIK* fast undesired movements can typically occur, in particular when subsequent suboptimal solutions are excessively far apart.

We also compared the computational cost of the two methods. The cycle time of our algorithm typically amounts to 0.38 ± 0.08 ms, while *CollisionIK* converges to the local optima in 0.27 ± 0.03 ms. It is worth mentioning that our algorithm does not approximate the robot with collision capsules as done in *CollisionIK*. We instead use convex meshes of the manipulator, improving accuracy in distance-based computations at the cost of slightly higher computational effort.

B. Real-world bi-manual teleoperation

We tested the robustness and feasibility of our algorithm on a real-world teleoperation platform. As shown in Fig. 3, the platform includes 2 Universal Robots UR5 manipulators and 2 Prensilia Mia Hand grippers (left and right models) [15]. The robot platform is controlled using the Perception Neuron motion capture suit running at 125 Hz.

52 participants teleoperated with the robot. Participants signed the informed consent and read the study information sheet. They were asked to manipulate soft spheres with a diameter of about 6 cm and, in particular, to transfer all the objects from the central box to the sides. To properly complete one transfer, they were required to 1) Grasp the object with

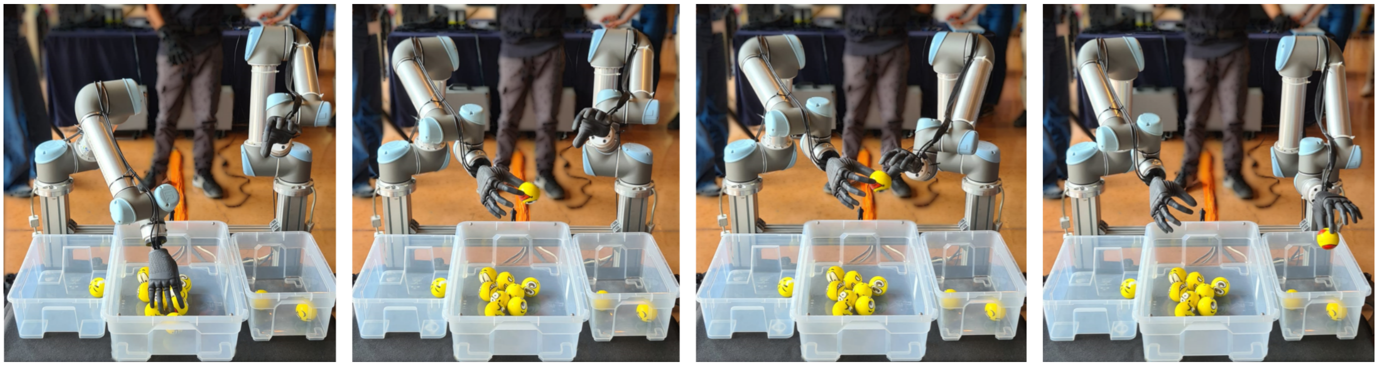

Fig. 3: The demonstration platform for our algorithm, which handles self-collisions and collisions with the boxes

one hand from the central box; 2) Move the object to the other hand; and 3) Place the object into the closest side box.

We used convex meshes both for the manipulators and for the anthropomorphic grippers. For the boxes, we used non-convex STL files instead. Our algorithm kept the same prediction horizon and loop rate as in the previous experiment, while we fixed the clearance parameter to 10 mm.

We compared raw inverse kinematics solutions with joint solutions obtained with our algorithm to estimate its total intervention time to avoid collisions, resulting in almost 20% of the total time. By post-processing joint data recorded from all demonstrations, we measured the closest point distance throughout the total intervention time.

Fig. 2b shows *clearance* violations, by reporting the instances where the closest point distance was below 10 mm, with median and IQR values of 8.8 ± 0.38 mm. The majority of critical violations of the safety margin given by the clearance parameter occur at the interaction of the right with the left fingers, suggesting that the reactive approach of updating the estimated pose of the gripper shapes at each initialisation of the constrained dynamics solver is in fact a suboptimal solution.

Fig. 2c shows the control cycle time. Typical median and IQR values are 1.1 ± 0.7 ms, which satisfies with sufficient margin the cycle time requirements given the 125 Hz loop rate.

IV. Conclusion

In the present work, we propose a novel local motion synthesis approach that solves the issue of attaining high pose tracking accuracy in collision-free sampled motion tracking. Our algorithm combines closed-loop inverse kinematics, rigid constrained dynamics and optimal control. We demonstrated in the simulation experiment that the *clearance* parameter allows us to easily regulate and precisely match the required safety margin with respect to obstacles. We also demonstrated the real-world feasibility of our algorithm for collision-safe sampled motion tracking in challenging scenarios. Future developments are envisioned to strictly meet cycle time requirements and to improve collision safety between grippers, which in the current solution are not properly considered as actuated parts in the constrained dynamics problem.

References

[1] M. M. Marinho, B. V. Adorno, K. Harada, and M. Mitsuishi, "Dynamic active constraints for surgical robots using vector-field inequalities," *IEEE Transactions on Robotics*, vol. 35, no. 5, pp. 1166–1185, 2019.

[2] S. Scherzinger, A. Roennau, and R. Dillmann, "Inverse kinematics with forward dynamics solvers for sampled motion tracking," in *2019 19th international conference on advanced robotics (ICAR)*. IEEE, 2019, pp. 681–687.

[3] G. Antonelli, "Stability analysis for prioritized closed-loop inverse kinematic algorithms for redundant robotic systems," *IEEE Transactions on Robotics*, vol. 25, no. 5, pp. 985–994, 2009.

[4] B. Siciliano, "Kinematic control of redundant robot manipulators: A tutorial," *Journal of intelligent and robotic systems*, vol. 3, pp. 201–212, 1990.

[5] N. Harrison, W. Liu, I. Jang, J. Carrasco, G. Herrmann, and N. Sykes, "A comparative study for obstacle avoidance inverse kinematics: Null-space based vs. optimisation-based," in *Towards Autonomous Robotic Systems: 21st Annual Conference, TAROS 2020, Nottingham, UK, September 16, 2020, Proceedings 21*. Springer, 2020, pp. 147–158.

[6] O. Khatib, "Real-time obstacle avoidance for manipulators and mobile robots," *The international journal of robotics research*, vol. 5, no. 1, pp. 90–98, 1986.

[7] D. Rakita, H. Shi, B. Mutlu, and M. Gleicher, "Collisionik: A per-instant pose optimization method for generating robot motions with environment collision avoidance," in *2021 IEEE International Conference on Robotics and Automation (ICRA)*. IEEE, 2021, pp. 9995–10 001.

[8] K. Van Wyk, M. Xie, A. Li, M. A. Rana, B. Babich, B. Peele, Q. Wan, I. Akinola, B. Sundaralingam, D. Fox *et al.*, "Geometric fabrics: Generalizing classical mechanics to capture the physics of behavior," *IEEE Robotics and Automation Letters*, vol. 7, no. 2, pp. 3202–3209, 2022.

[9] M. Spahn and J. Alonso-Mora, "Autotuning symbolic optimization fabrics for trajectory generation," in *2023 IEEE International Conference on Robotics and Automation (ICRA)*, 2023, pp. 11 287–11 293.

[10] N. Wilde, S. L. Smith, and J. Alonso-Mora, "Scalarizing multi-objective robot planning problems using weighted maximization," *IEEE Robotics and Automation Letters*, 2024.

[11] E. Catto, "Iterative dynamics with temporal coherence," in *Game developer conference*, vol. 2, no. 5, 2005.

[12] R. Featherstone, "A divide-and-conquer articulated-body algorithm for parallel o (log (n)) calculation of rigid-body dynamics. part 1: Basic algorithm," *The International Journal of Robotics Research*, vol. 18, no. 9, pp. 867–875, 1999.

[13] M. Ghazaei, A. Robertsson, and R. Johansson, "Online minimum-jerk trajectory generation," in *2015 IMA Conference on Mathematics of Robotics*, 2015.

[14] A. Colomé and C. Torras, "Redundant inverse kinematics: Experimental comparative review and two enhancements," in *2012 IEEE/RSJ International Conference on Intelligent Robots and Systems*. IEEE, 2012, pp. 5333–5340.

[15] M. Controzzi, F. Clemente, D. Barone, A. Ghionzoli, and C. Cipriani, "The sssa-myhand: a dexterous lightweight myoelectric hand prosthesis," *IEEE Transactions on Neural Systems and Rehabilitation Engineering*, vol. 25, no. 5, pp. 459–468, 2016.